Pergamon

J. Biomechanics, Vol. 27, No. 5, pp. 551–569, 1994
Elsevier Science Ltd

0021-9290/94 $6.00+.00

A FINITE ELEMENT MUSCULOSKELETAL MODEL OF THE SHOULDER MECHANISM

F. C. T. VAN DER HELM

Man–Machine Systems Group, Laboratory for Measurement and Control, Department of Mechanical Engineering, Delft University of Technology, Delft, The Netherlands

Abstract—The finite element method described in this study provides an easy method to simulate the kinetics of multibody mechanisms. It is used in order to develop a musculoskeletal model of the shoulder mechanism. Each relevant morphological structure has been represented by an appropriate element. For the shoulder mechanism two special-purpose elements have been developed: a SURFACE element representing the scapulothoracic gliding plane and a CURVED-TRUSS element to represent muscles which are wrapped around bony contours. The model contains four bones, three joints, three extracapsular ligaments, the scapulothoracic gliding plane and 20 muscles and muscle parts. In the model, input variables are the positions of the shoulder girdle and humerus and the external load on the humerus. Output variables are muscle forces subject to an optimization procedure in which the mechanical stability of the glenohumeral joint is one of the constraints. Four different optimization criteria are compared. For 12 muscles, surface EMG is used to verify the model. Since the optimum muscle length and force–length relationship are unknown, and since maximal EMG amplitude is length dependent, verification is only possible in a qualitative sense. Nevertheless, it is concluded that a detailed model of the shoulder mechanism has been developed which provides good insight into the function of morphological structures.

INTRODUCTION

The shoulder mechanism, which consists of thorax, clavicula, scapula and humerus, is because of its complexity one of the most challenging systems in musculoskeletal modelling. Motions of the upper arm are the result of the simultaneous motions in the sternoclavicular, acromioclavicular and glenohumeral joints. External load and inertia forces of the upper extremity are transmitted to the thorax through the muscles crossing these joints and through the bones of the shoulder girdle. The scapula provides a moveable but stable base for a large range of motion of the humerus. Motion studies have revealed that a fixed and reproducible relation exists between motions of the scapula and the humerus, the so-called spinohumeral rhythm (Inman *et al.*, 1944; Pronk, 1987).

Motions of the scapula are constrained on the one hand by the so-called scapulothoracic gliding plane, which connects the medial border of the scapula to the thorax, and on the other hand by the clavicula, which allows the acromion to move more or less on a sphere around the sternoclavicular joint. Due to these constraints, the shoulder girdle is a closed-chain mechanism. For this reason, models of the shoulder mechanism, or even only the glenohumeral joint, should not be restricted to two dimensions. Furthermore, motions are constrained by three extracapsular ligaments, i.e. the costoclavicular, conoid and trapezoid ligaments. Seventeen muscles are crossing the three joints of the shoulder mechanism. They are listed in Table 1. Muscles running from the thorax to the scapula are crossing two joints, and muscles running from the thorax directly to the humerus, like m. latissimus dorsi and m. pectoralis major, are even crossing three joints. Most of these muscles have large attachment sites, are broad and flat, and have multidirectional muscle bundles.

The complexity of the shoulder mechanism is probably the reason that thus far hardly any three-dimensional models were developed. Mollier (1899), Shiino (1913) and Hvorslev (1927) used human specimens to build physical models of the shoulder mechanism (Fig. 1). They replaced the muscles by cords and connected them to a keyboard. Then, by pressing the keys a motion could be established and, in reverse, when moving the bones the deviation of the keys could be observed to measure the length changes of the muscles. These models were essentially kinematic.

Subsequently, two-dimensional biomechanical models started to dominate the research of the shoulder mechanism. These models merely described the motion of the humerus with respect to a nonmoving scapula (DeLuca and Forrest, 1973; Dul, 1987; Poppen and Walker, 1978). Due to the oversimplification, these models did not add much to the comprehension and understanding of the entire system.

Three-dimensional models are scarce. Karlsson and coworkers (Karlsson, 1990; Karlsson and Peterson, 1992; Karlsson *et al.*, 1989) used a Newton–Euler approach and three-dimensional roentgenographic motion recording for modelling of the shoulder mechanism. Apparent problems in this approach are caused by the closed-chain nature of the mechanism, due to the scapulothoracic gliding plane and polyarticular muscles. In Karlsson and Peterson only results of glenohumeral muscles have been presented. Wood

Received in final form 10 *June* 1993.

Table 1. Muscles of the shoulder mechanism

Thoracoscapular muscles	Thoracohumeral muscles	Scapulohumeral muscles
m. trapezius*	m. latissimus dorsi	m. deltoideus‡
m. levator scapulae	m. pectoralis major‡	m. coracobrachialis
m. rhomboideus		m. teres major
m. pectoralis minor		m. teres minor
m. subclavius†		m. infraspinatus
m. serratus anterior		m. supraspinatus
		m. subscapularis
		m. triceps, c. longum§
		m. biceps§

* Partly inserting at clavicula.
† Inserting at clavicula.
‡ Partly originating at clavicula.
§ Inserting at forearm bones.

et al. (1989) described a model based on a Lagrangian approach, but did not elaborate on the necessary equations. Both modelling approaches did not present much details thus far, so it is not clear if important features of the shoulder mechanism are included, e.g. motion of both scapula and humerus, change of moment arms due to this motion, constraints of the scapulothoracic gliding plane and the stability of the glenohumeral joint.

Due to the complexity of the shoulder mechanism, there is little or no insight into the mechanics constituting its motion behavior and the function of muscles and ligaments. Hence, the interpretation of complaints in the shoulder region is hampered and often does not result in a detailed diagnosis. Surgery in the shoulder region is often based on a misjudgement of the underlying mechanics. The main motive of this study was to develop a model of the shoulder mechanism by which it would be possible to gain insight into the function of morphological structures. Results of this analysis can, for instance, be applied to predict optimal fusion angles for a glenohumeral arthrodesis, to improve the application of an endoprosthesis, or to develop therapies for patients with a habitual glenohumeral subluxation.

Nowadays a schism is encountered in deriving motion equations for multibody systems (Sol, 1983). Biomechanical models have grown so complex that analytical solutions are very hard to obtain, so numerical solutions are preferred with the appearance of more and more powerful computers. In order to model the shoulder mechanism a computer program SPACAR is used, based on the finite element method and specially suited for the dynamic analysis of multibody mechanisms. At each position of the mechanism, motion equations are numerically derived based on deformations of the elements and displacements of its nodes. A special feature of this finite element method is that the subsequent position of the mechanism, as determined by generalized coordinates, is calculated iteratively.

In this article a summary of the finite element method will be presented. Detailed information can be found in van der Werff (1977), van der Werff and Jonker (1983), Schwab (1983) and Jonker (1988). Subsequently, a few elements specially developed for the shoulder mechanism are introduced and discussed in more detail. The shoulder model in terms of finite elements is presented. Results of this study will be compared with EMG recordings of the shoulder.

FINITE ELEMENT METHOD

The gross morphological structures of the shoulder mechanism can be represented by finite elements of a simple geometry. Since the mechanical properties of these elements are well defined, the kinematic and dynamic behavior of the whole mechanism can be simulated. Characteristic for this finite element method is that deformation modes of the elements are expressed as a function of the displacements of its endpoint nodes. There are two types of nodes (position nodes and orientation nodes) and three basic types of elements (TRUSS elements, HINGE elements and BEAM elements). The TRUSS element has two position nodes and one deformation mode: elongation, calculated by the change in distance between both position nodes. The HINGE element has two orientation nodes and three deformation modes: torsion around its initial axis and two bending deformations of this axis. The BEAM element has two position nodes and two orientation nodes, and six deformation modes: elongation, torsion around the length axis of the BEAM and two bending deformations of each endpoint of the BEAM. Contact between elements is obtained by letting them share common nodes. For instance, two BEAM elements rotate around a HINGE defined in between if the orientation nodes of the HINGE are identical to the orientation nodes of connected endpoints of the BEAM elements.

New elements

SURFACE elements. The scapulothoracic gliding plane imposes constraints on the scapular motions, which turns the shoulder girdle into a closed-chain

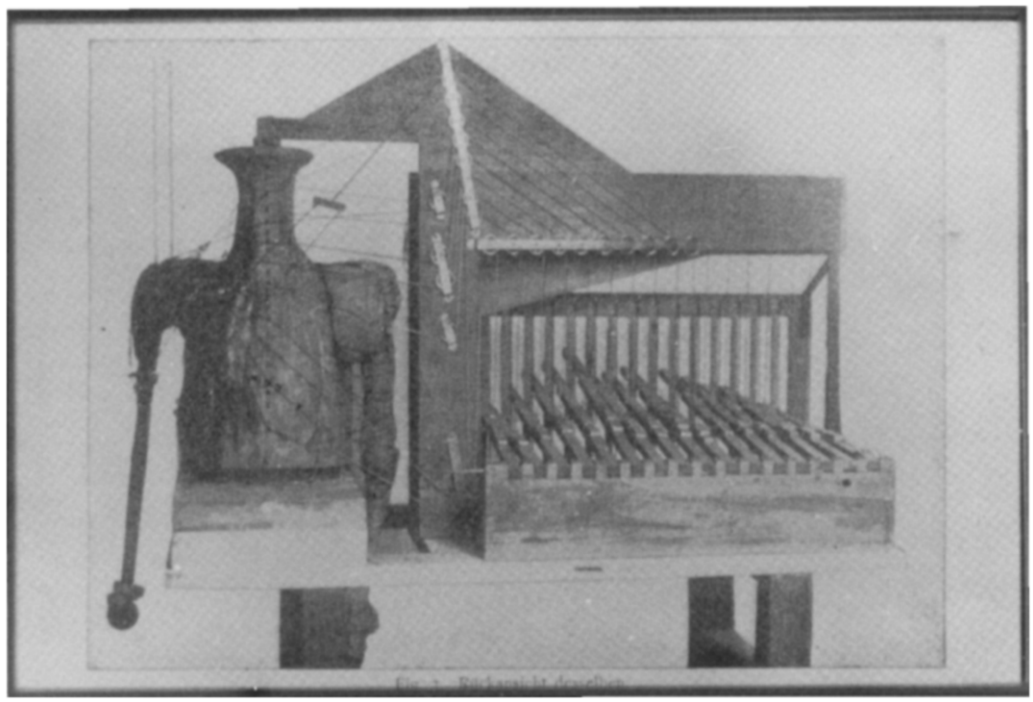

Fig. 1. Shoulder 'organ', built by Mollier (1899). Muscles have been replaced by cords. The mechanism can be moved by pressing the keys, which result in 'contraction' of the muscles.

mechanism. Reaction forces exerted by the thorax at the scapula are important for the force and moment balance of the sternoclavicular and acromioclavicular joints. In the shoulder model the scapulothoracic gliding plane is represented by two SURFACE elements, one near the trigonum spinae (TS) and one near the angulus inferior (AI). In this way it is assured that the medial border of the scapula is connected to the thorax. The SURFACE element has been described by Pronk (1989) for kinematic purposes. Of late, this element was adapted such that it could be used for dynamic analysis as well. The SURFACE element has one position node and, in addition, a parameter description of the surface area to which the node is attached. It has one deformation mode: the distance between the node and the surface.

Pronk and van der Padt (1986), van der Helm *et al.* (1992) and Pronk (1991) showed that the thorax can be modelled by an ellipsoid. The distance from a point to the ellipsoid is calculated iteratively along the normal vector to the ellipsoid through this point (Appendix A). The first and second derivatives of this deformation are calculated from the normal vector. To ensure that the point is attached to the surface, the deformation should be zero. The stress in this SURFACE element, i.e. the force exerted by the node at the surface, will be directed along the normal vector. During the optimization procedure this force will be constrained such that only compression can occur.

CURVED-TRUSS element. A number of muscles in the shoulder region wrap around underlying morphological structures, i.e. bony contours. There are basically two methods to represent these muscles. The first method is to use the centroid line for estimation of the muscle line of action. The main disadvantage of this method is that it is only applicable to one position of the model. The method used in the current model is the bony contour method. The muscle line of action is the shortest distance between the origin and the insertion around the bony contour, which is in between. The effective moment arm of the muscle can be calculated from the straight line between one attachment and the tangent point at the bony contour. For any position of the mechanism this line can be calculated and is represented by a special element, the CURVED-TRUSS element. The CURVED-TRUSS element has three nodes: the origin, insertion and tangent point constituting the effective muscle line of action. After each step the tangent points are calculated again. The only deformation is elongation of the element, calculated from the length of the element around the bony contour. The first and second derivatives of the element are calculated from the straight line between one attachment and its tangent point. Three representations of bony contours are used in the shoulder model: a sphere (caput humeri; the combined tuberculum majus and minus), a cylinder (collum humeri) and an ellipsoid (thorax). For a sphere the tangent point can be calculated analytically, depending on the known position of the origin, insertion and center and radius of the sphere. For the cylinder and ellipsoid the tangent points were approximated iteratively (van der Helm, 1993). Appendix B describes the calculation of the deformation and derivatives of the CURVED-TRUSS element.

Model simulations. Motion of the mechanism is expressed in terms of the motion of generalized coordinates, comparable to the Lagrangian approach. These generalized coordinates can be position coordinates or deformation modes. The model can be used for an inverse dynamic analysis as well as a dynamic analysis. In the inverse dynamic analysis the most common input variables of biomechanical models can be used: either the position of bony landmarks and/or the angle between two segments which is expressed as torsion around the initial axis of a HINGE element. Output variables are muscle forces calculated using an optimization criterion like minimization of the sum of squared muscle forces for minimization of the sum of squared muscle stresses.

For forward dynamic simulations in the near future, a third-order muscle model based on the work of Winters and Stark (1985) has been developed linking the neural input for each muscle to the generated force of an active element. These muscle forces in combination with inertia and external load of the system result in the motion of the mechanism.

Kinematic analysis

The position of the mechanism is fully determined by independent generalized coordinates. The central point in the kinematic analysis is the calculation of the new position of the mechanism as a function of these generalized coordinates. The number of generalized coordinates is equal to the number of degrees of freedom (DOF) of the mechanism. Generalized coordinates can consist of position coordinates and deformation modes. Then, starting from position i, the next position $(i+1)$ is approximated by a second-order Taylor expansion:

$$\mathbf{x}_{i+1} = \mathbf{x}_i + \mathrm{D}F^x \cdot (\Delta\mathbf{x}^m, \Delta\mathbf{e}^m) + \tfrac{1}{2}(\mathrm{D}^2F^x \cdot (\Delta\mathbf{x}^m, \Delta\mathbf{e}^m)) \cdot (\Delta\mathbf{x}^m, \mathbf{e}^m), \quad (1)$$

where $\mathbf{x}$ is the vector with position and orientation coordinates, $(\Delta\mathbf{x}^m, \Delta\mathbf{e}^m)$ is the column vector describing the change of generalized coordinates, position coordinates $(\Delta\mathbf{x}^m = \mathbf{x}^m_{i+1} - \mathbf{x}^m_i)$ and deformation modes $(\Delta\mathbf{e}^m = \mathbf{e}^m_{i+1} - \mathbf{e}^m_i)$, respectively, $\mathrm{D}F^x$ is the matrix of first derivatives of coordinate vector $\mathbf{x}$ with respect to the column vector of generalized coordinates: $\delta\mathbf{x}/(\delta\mathbf{x}^m, \delta\mathbf{e}^m)$, in which $(\delta\mathbf{x}^m, \delta\mathbf{e}^m) = [\delta\mathbf{x}^{mT}\ \delta\mathbf{e}^{mT}]^T$ (superscript T means transpose), and D^2F^x is the matrix of second derivatives of coordinate vector $\mathbf{x}$ with respect to the vector of generalized coordinates: $\delta^2\mathbf{x}/((\delta\mathbf{x}^m, \delta\mathbf{e}^m) \cdot (\delta\mathbf{x}^m, \delta\mathbf{e}^m)^T)$. D^2F^x is a matrix with three dimensions.

At each position i the matrices $\mathrm{D}F^x$ and D^2F^x, the first- and second-order geometric transfer functions, respectively, can be calculated from the position and

deformation of the elements. First the zero-order geometric transfer function is established. This is the nonlinear function D of the vector of deformations $\mathbf{e}$ and the vector of position and orientation coordinates $\mathbf{x}$:

$$\mathbf{e}=D(\mathbf{x}). \tag{2}$$

The function in equation (2) can be differentiated with respect to the generalized coordinates, yielding the first-order geometric transfer function:

$$\mathrm{D}F^{e}=\mathrm{D}D\cdot\mathrm{D}F^{x}, \tag{3}$$

where $\mathrm{D}D$ is a matrix containing derivatives of the vector of deformations $\mathbf{e}$ with respect to the vector of coordinates $\mathbf{x}$: $\delta\mathbf{e}/\delta\mathbf{x}^{\mathrm{T}}$. $\mathrm{D}F^{e}$ is a matrix of first derivatives of the vector of deformations $\mathbf{e}$ with respect to generalized coordinates $(\delta\mathbf{e}/\delta\mathbf{x}^{\mathrm{m}}, \delta\mathbf{e}^{\mathrm{m}})$.

Depending on the constraint conditions and the choice of the generalized coordinates, the vector of position coordinates $\mathbf{x}$ and element deformations $\mathbf{e}$ can be divided into three parts:

- $\mathbf{x}^{\mathrm{o}}$ vector of fixed support coordinates,
- $\mathbf{x}^{\mathrm{c}}$ vector of dependent nodal coordinates,
- $\mathbf{x}^{\mathrm{m}}$ vector of global generalized coordinates,
- $\mathbf{e}^{\mathrm{o}}$ vector of fixed prescribed deformation mode coordinates,
- $\mathbf{e}^{\mathrm{m}}$ vector of relative generalized coordinates,
- $\mathbf{e}^{\mathrm{c}}$ vector of dependent deformation mode coordinates,

and analogously to this partitioning

$$\begin{bmatrix}\mathrm{D}F^{eo}\\ \mathrm{D}F^{em}\\ \mathrm{D}F^{ec}\end{bmatrix}=\begin{bmatrix}\mathrm{D}^{\mathrm{o}}D^{\mathrm{o}} & \mathrm{D}^{\mathrm{c}}D^{\mathrm{o}} & \mathrm{D}^{\mathrm{m}}D^{\mathrm{o}}\\ \mathrm{D}^{\mathrm{o}}D^{\mathrm{m}} & \mathrm{D}^{\mathrm{c}}D^{\mathrm{m}} & \mathrm{D}^{\mathrm{m}}D^{\mathrm{m}}\\ \mathrm{D}^{\mathrm{o}}D^{\mathrm{c}} & \mathrm{D}^{\mathrm{c}}D^{\mathrm{c}} & \mathrm{D}^{\mathrm{m}}D^{\mathrm{c}}\end{bmatrix}\cdot\begin{bmatrix}\mathrm{D}F^{xo}\\ \mathrm{D}F^{xc}\\ \mathrm{D}F^{xm}\end{bmatrix}, \tag{4}$$

in which the following matrices are known by definition:

$$\begin{aligned}\mathrm{D}F^{eo}&=\left[\frac{\delta\mathbf{e}^{\mathrm{o}}}{\delta\mathbf{x}^{\mathrm{m}}},\frac{\delta\mathbf{e}^{\mathrm{o}}}{\delta\mathbf{e}^{\mathrm{m}}}\right]=[\mathbf{0},\mathbf{0}],\\ \mathrm{D}F^{em}&=\left[\frac{\delta\mathbf{e}^{\mathrm{m}}}{\delta\mathbf{x}^{\mathrm{m}}},\frac{\delta\mathbf{e}^{\mathrm{m}}}{\delta\mathbf{e}^{\mathrm{m}}}\right]=[\mathbf{0},\mathbf{I}],\\ \mathrm{D}F^{xo}&=\left[\frac{\delta\mathbf{x}^{\mathrm{o}}}{\delta\mathbf{x}^{\mathrm{m}}},\frac{\delta\mathbf{x}^{\mathrm{o}}}{\delta\mathbf{e}^{\mathrm{m}}}\right]=[\mathbf{0},\mathbf{0}],\\ \mathrm{D}F^{xm}&=\left[\frac{\delta\mathbf{x}^{\mathrm{m}}}{\delta\mathbf{x}^{\mathrm{m}}},\frac{\delta\mathbf{x}^{\mathrm{m}}}{\delta\mathbf{e}^{\mathrm{m}}}\right]=[\mathbf{I},\mathbf{0}].\end{aligned} \tag{5}$$

The unknown matrices $\mathrm{D}F^{ec}$ and $\mathrm{D}F^{xc}$ can be calculated. The second-order geometric transfer functions D^2F^{ec} and D^2F^{xc} can be obtained analogously by differentiating equation (3) with respect to the generalized coordinates once again.

After the first approximation of the new position $(i+1)$ of the mechanism is obtained, an iteration process based on the Newton–Raphson method is applied to guarantee that ultimately (Jonker, 1988)

$$\mathbf{e}_{i+1}=D(\mathbf{x}_{i+1}). \tag{6}$$

Finally the velocity and acceleration of the nodal coordinates can be calculated from the velocity and acceleration of the generalized coordinates:

$$\begin{aligned}\dot{\mathbf{x}}&=\mathrm{D}F^{x}\cdot(\dot{\mathbf{x}}^{\mathrm{m}},\dot{\mathbf{e}}^{\mathrm{m}}),\\ \dot{\mathbf{e}}&=\mathrm{D}F^{e}\cdot(\dot{\mathbf{x}}^{\mathrm{m}},\dot{\mathbf{e}}^{\mathrm{m}}),\end{aligned} \tag{7}$$

$$\ddot{\mathbf{x}}=(\mathrm{D}^2F^{x}\cdot(\dot{\mathbf{x}}^{\mathrm{m}},\dot{\mathbf{e}}^{\mathrm{m}}))\cdot(\dot{\mathbf{x}}^{\mathrm{m}},\dot{\mathbf{e}}^{\mathrm{m}})+\mathrm{D}F^{x}\cdot(\ddot{\mathbf{x}}^{\mathrm{m}},\ddot{\mathbf{e}}^{\mathrm{m}}),$$

$$\ddot{\mathbf{e}}=(\mathrm{D}^2F^{e}\cdot(\dot{\mathbf{x}}^{\mathrm{m}},\dot{\mathbf{e}}^{\mathrm{m}}))\cdot(\dot{\mathbf{x}}^{\mathrm{m}},\dot{\mathbf{e}}^{\mathrm{m}})+\mathrm{D}F^{e}\cdot(\ddot{\mathbf{x}}^{\mathrm{m}},\ddot{\mathbf{e}}^{\mathrm{m}}). \tag{8}$$

Dynamic analysis

In the dynamic analysis, motion equations of the mechanism are derived by using Lagrange's form of d'Alembert's principle. In this approach, a virtual power approach, the computational advantages of the Newton–Euler and Lagrange's equations are combined, i.e. the advantage of eliminating nonworking constraint forces without the need of elaborate differentiation of the energy equations. The final number of equations is equal to the number of DOF of the mechanism. These differential equations can be integrated using an appropriate integration algorithm.

To obtain the motion equations the principle of virtual power for the vectors $\mathbf{f}$ of external forces and $\mathbf{f}_{\mathrm{in}}$ for inertia forces, and for vector $\boldsymbol{\sigma}$ of stress associated with the deformation of the elements can be written in the form

$$\langle\dot{\mathbf{e}},\boldsymbol{\sigma}\rangle=\langle\dot{\mathbf{x}},(\mathbf{f}-\mathbf{f}_{\mathrm{in}})\rangle\Rightarrow\dot{\mathbf{e}}^{\mathrm{T}}\cdot\boldsymbol{\sigma}=\dot{\mathbf{x}}^{\mathrm{T}}\cdot(\mathbf{f}-\mathbf{f}_{\mathrm{in}}), \tag{9}$$

where the notation $\langle\ ,\ \rangle$ is the scalar product of two vectors and where

$$\begin{aligned}\dot{\mathbf{e}}&=\mathrm{D}F^{e}\cdot(\dot{\mathbf{x}}^{\mathrm{m}},\dot{\mathbf{e}}^{\mathrm{m}}),\\ \dot{\mathbf{x}}&=\mathrm{D}F^{x}\cdot(\dot{\mathbf{x}}^{\mathrm{m}},\dot{\mathbf{e}}^{\mathrm{m}}).\end{aligned}$$

Since equation (9) is true for every value of $(\dot{\mathbf{x}}^{\mathrm{m}},\dot{\mathbf{e}}^{\mathrm{m}})$ it can be reduced to

$$\mathrm{D}F^{e\mathrm{T}}\cdot\boldsymbol{\sigma}=\mathrm{D}F^{x\mathrm{T}}\cdot(\mathbf{f}-\mathbf{f}_{\mathrm{in}}). \tag{10}$$

Inertia in the system is included by subtracting inertia forces $(\mathbf{f}_{\mathrm{in}})$ using d'Alembert's principle. Since in the shoulder model only rigid BEAM elements are used and the attribution of muscle mass to inertia forces is neglected, inertia in the system can be included using a lumped mass representation at the position and orientation nodes, representing translational and rotational inertia, respectively. Then, with equation (8),

$$\begin{aligned}\mathbf{f}_{\mathrm{in}}&=\mathbf{M}\cdot\ddot{\mathbf{x}}\\ &=\mathbf{M}\cdot\{(\mathrm{D}^2F^{x}\cdot(\dot{\mathbf{x}}^{\mathrm{m}},\dot{\mathbf{e}}^{\mathrm{m}}))\cdot(\dot{\mathbf{x}}^{\mathrm{m}},\dot{\mathbf{e}}^{\mathrm{m}})\\ &\quad+\mathrm{D}F^{x}\cdot(\ddot{\mathbf{x}}^{\mathrm{m}},\ddot{\mathbf{e}}^{\mathrm{m}})\},\end{aligned} \tag{11}$$

where $\mathbf{M}$ is the system mass matrix describing the lumped rotational and translational inertia at the orientation and position nodes, respectively.

Substitution of equation (11) into equation (10) results in the motion equations:

$$DF^{x\mathrm{T}}\cdot\mathbf{M}\cdot DF^{x}\cdot(\ddot{\mathbf{x}}^{m},\ddot{\mathbf{e}}^{m})=-DF^{e\mathrm{T}}\cdot\boldsymbol{\sigma}+DF^{x\mathrm{T}}\cdot\mathbf{f}$$
$$-DF^{x\mathrm{T}}\cdot\mathbf{M}\cdot(D^{2}F^{x}(\dot{\mathbf{x}}^{m},\dot{\mathbf{e}}^{m}))\cdot(\dot{\mathbf{x}}^{m},\dot{\mathbf{e}}^{m}). \quad (12)$$

Equation (12) describes a number of differential equations equal to the number of generalized coordinates as depicted by the vector $(\Delta\mathbf{x}^{m},\Delta\mathbf{e}^{m})$. The motion equations can be solved numerically by using one of the standard numerical integration routines. In this finite element method a predictor/corrector method with variable order and step-size is used (Shampine and Gordon, 1975). However, in the inverse dynamic analysis as used in the shoulder mechanism model, motion equations are reduced to algebraic equations.

After solving the motion equations a kinetostatic analysis is performed in order to calculate the internal stress distribution and the unknown reaction forces of the mechanism. After substituting equation (3) into equation (10) the next equation is obtained:

$$DD^{\mathrm{T}}\cdot\boldsymbol{\sigma}=\mathbf{f}-\mathbf{f}_{in}. \quad (13)$$

Analogously to equation (4) this can be split into

$$\begin{bmatrix} D^{o}D^{o\mathrm{T}} & D^{o}D^{m\mathrm{T}} & D^{o}D^{c\mathrm{T}} \\ D^{c}D^{o\mathrm{T}} & D^{c}D^{m\mathrm{T}} & D^{c}D^{c\mathrm{T}} \\ D^{m}D^{o\mathrm{T}} & D^{m}D^{m\mathrm{T}} & D^{m}D^{c\mathrm{T}} \end{bmatrix}\cdot\begin{bmatrix}\boldsymbol{\sigma}^{o}\\ \boldsymbol{\sigma}^{m}\\ \boldsymbol{\sigma}^{c}\end{bmatrix}\cdot\begin{bmatrix}\mathbf{f}^{o}\\ \mathbf{f}^{c}-\mathbf{f}^{c}_{in}\\ \mathbf{f}^{m}-\mathbf{f}^{m}_{in}\end{bmatrix}, \quad (14)$$

where $\boldsymbol{\sigma}^{o}$ is the vector of stresses attributed to fixed deformations, $\boldsymbol{\sigma}^{m}$ is the vector of driving stresses attributed to generalized deformations, $\boldsymbol{\sigma}^{c}$ is the vector of stresses calculable from dependent deformation mode coordinates, $\mathbf{f}^{o}$ is the vector of reaction forces at fixed coordinates, $\mathbf{f}^{m}$ is the vector of driving forces at generalized coordinates and $\mathbf{f}^{c}$ is the vector of prescribed (external) forces.

The stress components $\boldsymbol{\sigma}^{o}$ and $\boldsymbol{\sigma}^{m}$ can be calculated:

$$\begin{bmatrix}\boldsymbol{\sigma}^{o}\\ \boldsymbol{\sigma}^{m}\end{bmatrix}=[D^{c}D^{o\mathrm{T}}\ D^{c}D^{m\mathrm{T}}]^{-1}\cdot(\mathbf{f}^{c}-\mathbf{f}^{c}_{in}-D^{c}D^{c\mathrm{T}}\cdot\boldsymbol{\sigma}^{c}), \quad (15)$$

where vector $\boldsymbol{\sigma}^{c}$ is calculated from constitutive equations relating the deformations of the element to stress:

$$\boldsymbol{\sigma}^{c}=\mathbf{C}\cdot\mathbf{e}^{c}+\mathbf{K}\cdot\dot{\mathbf{e}}^{c}, \quad (16)$$

in which $\mathbf{C}$ is the system stiffness matrix and $\mathbf{K}$ is the system damping matrix. Any other user-supplied (nonlinear) constitutive equation can be used in this equation. Finally the vector of reaction forces $\mathbf{f}^{o}$ and the vector of driving forces $\mathbf{f}^{m}$ can be calculated from equation (14).

Inverse dynamic optimization

Input variables of the model are the prescribed motion of the mechanism, expressed in position, velocity and acceleration of generalized coordinates $(\Delta\mathbf{x}^{m},\Delta\mathbf{e}^{m})$. In the kinematic analysis, length, velocity and acceleration of muscles can be calculated. In the inverse dynamic analysis, force vector $\mathbf{f}^{m}$ and stress vector $\boldsymbol{\sigma}^{m}$ are calculated as driving forces, attributed to the generalized coordinates. In fact, driving forces for this motion are generated by muscles. Hence, driving forces $\mathbf{f}^{m}$ and $\boldsymbol{\sigma}^{m}$ are distributed over the stress vector associated with the stress in the active TRUSS and CURVED-TRUSS elements representing the muscles. Subsequently, in the kinetostatic analysis this muscle stress will result in forces at the endnodes in the direction of the element. Thus, the course of the muscle element can in fact be viewed as the muscle line of action, exerting force at its attachments on the bone. One unit of stress in the muscle element results in one unit of force at both attachments.

In the kinematic analysis, deformation modes of the active elements are part of the deformation vector $\mathbf{e}^{c}$. The associated stress vector $\boldsymbol{\sigma}^{c}$ is split into two parts: $\boldsymbol{\sigma}^{c1}$ for the passive dependent stresses and $\boldsymbol{\sigma}^{c2}$ for the active stresses, to be calculated in the inverse dynamic analysis. However, since in general there are more active elements than DOF, the solution for $\boldsymbol{\sigma}^{c2}$ is indeterminate. Therefore, this vector $\boldsymbol{\sigma}^{c2}$ is calculated in an optimization procedure with an adequate optimization criterion, whereas equality constraints from the motion equations have to be considered. From the motion equations [equation (12)] the relation between active stresses $\boldsymbol{\sigma}^{c2}$ on the one hand and driving forces $\mathbf{f}^{m}$ and driving stresses $\boldsymbol{\sigma}^{m}$ of the generalized coordinates on the other can be derived:

$$DF^{ec2\mathrm{T}}\cdot\boldsymbol{\sigma}^{c2}=-DF^{em}\cdot\boldsymbol{\sigma}^{m}+DF^{xm\mathrm{T}}\cdot(\mathbf{f}^{m}-\mathbf{f}^{m}_{in}). \quad (17)$$

Substituting equation (5) into equation (17) results in

$$DF^{ec2\mathrm{T}}\cdot\boldsymbol{\sigma}^{c2}=\begin{bmatrix}(\mathbf{f}^{m}-\mathbf{f}^{m}_{in})\\ -\boldsymbol{\sigma}^{m}\end{bmatrix}. \quad (18)$$

Equation (18) describes the equality constraints for the optimization procedure due to the motion equations.

Example: In this equation the matrix $DF^{ec2\mathrm{T}}$ is the derivative of the elongation of the muscle elements with respect to the degrees of freedom $(\delta\mathbf{e}^{c2}/(\delta\mathbf{x}^{m},\delta\mathbf{e}^{m}))$. If the rotations $\boldsymbol{\phi}$ of the joint are the DOF, then $\boldsymbol{\sigma}^{m}$ corresponds to the vector of net joint moments and $\delta\mathbf{e}^{c2}/(\delta\mathbf{x}^{m},\delta\mathbf{e}^{m})$ is analogous to the definition of An *et al.* (1984) for moment arm a of a muscle: $a=\delta l/\delta\phi$.

Then equation (18) can be compared with

$$\sum_{i} a_{i}\cdot F_{i}=M,$$

where a_{i} is the moment arm of muscle i, F_{i} is the force attributed to muscle i and M is the net joint moment.

Furthermore, additional constraints to the optimization procedure can be imposed, e.g. the constraint that at the SURFACE elements of the scapulothoracic gliding plane only compression forces can occur and that only traction forces in the ligaments

exists. Special constraints to the joint reaction forces in the glenohumeral joint will be explained later.

In the kinetostatic equations these constraints exist in the form of limitations on particular items of the σ^o vector. If σ^o is zero no stresses occur, if σ^o is smaller than zero compression forces occur, and if σ^o is greater than zero traction forces occur. For example, forces in the SURFACE elements are restricted to compression forces, and forces in the ligaments are restricted to traction forces. The relation between these items of σ^o and the variables σ^{c2} in the optimization procedure can be established according to equation (15):

$$[D^c D^{oT}\ D^c D^{mT}]^{-1} \cdot D^c D^{c2T} \cdot \sigma^{c2} = -\begin{bmatrix}\sigma^o \\ \sigma^m\end{bmatrix} + [D^c D^{oT}\ D^c D^{mT}]^{-1} \cdot (f^c - f^c_{in} - D^c D^{c1T} \cdot \sigma^{c1}). \quad (19)$$

Furthermore, muscle forces are constrained such that the joint reaction force vector of the glenohumeral joint intersects the glenoid. This nonlinear constraint is explained in more detail in the constraints section and Appendix C.

Finally, each element of the vector σ^{c2} is constrained to be greater than zero (only traction forces) and smaller than the maximal force which can be exerted by the muscle element depending on the physiological cross-sectional area of the muscle. For the optimization procedure a gradient-based algorithm has been used, which included linear and nonlinear equations and inequalities (NAG-library routine E04UCF, Numerical Algorithms Group Inc., Downers Grove, Il).

MODEL OF THE SHOULDER MECHANISM

In Fig. 2 the inverse dynamic model of the shoulder mechanism is depicted in a block diagram. Input variables to the model are position, velocity and acceleration of generalized coordinates and external forces. Output variables of the model consist of muscle forces calculated by using an optimization criterion. The model itself consists of motion equations describing the mechanical behavior of the shoulder mechanism, derived by using the finite element method.

Parameters for the model have been derived in an extensive cadaver study consisting of both shoulders of seven cadavers. There are three types of parameters: inertia parameters describing the translational and rotational inertia of the segments, muscle contraction parameters describing the maximal force attributed to a muscle element depending on the physiological cross-sectional area (PCSA) of the muscle, and geometry parameters describing the position of joint rotation centers, muscle and ligament attachments, shape and position of bony contours and the position of bony landmarks to link the recorded motion of subjects to motions of the model. In this study, parameters derived at the right shoulder of a more or less

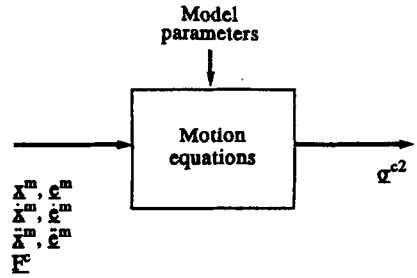

Fig. 2. Block diagram of the model of the shoulder mechanism. Input variables are the position (and velocity and acceleration) of the bones (x^m, e^m and derivatives) and the external load (F^e). Output variables are muscle forces (σ^{c2}). Model parameters describe the shoulder morphology.

median cadaver are used. The complete cadaver experiment, including all geometric data used in the present model, has been described elsewhere (van der Helm *et al.*, 1992; van der Helm and Veenbaas, 1991; Veeger *et al.*, 1991).

Elements

The sternoclavicular (SC) joint between the sternum and the clavicula is represented as a spherical joint by three orthogonal HINGE elements. A BEAM representing the clavicula connects this joint with the acromioclavicular (AC) joint between the clavicula and the scapula, also modelled as a spherical joint. The scapula is represented by two rigidly connected BEAM elements: one from the AC joint to trigonum spinae (TS) at the medial border of the scapula and the other from TS to angulus inferior (AI). TS and AI are connected with SURFACE elements to the thorax. The glenohumeral (GH) joint is connected to the AC joint by another BEAM rigidly connected with the scapula. The humerus, and the rest of the arm, is represented by a BEAM from the GH joint to the midpoint between the medial and lateral epicondyle. The mechanism consisting of the clavicula, scapula, humerus and the scapulothoracic gliding plane, with three spherical joints, has seven DOF: four at the shoulder girdle and three for the humerus. Ligaments are modelled as flexible TRUSS elements. Attachment points of these elements are rigidly connected with BEAM elements to the respective bones. Three extracapsular ligaments are accounted for in the model: the costoclavicular ligament crossing the SC joint and the conoid and trapezoid ligaments crossing the AC joint. The mechanism described so far is shown in Fig. 3, with a few muscle elements added.

Muscles are modelled as active elements: TRUSS or CURVED-TRUSS elements. Mostly, more than one element is necessary for adequately representing the mechanical effect of muscles with large attachment sites. Each muscle is represented by one to six elements, where each element can be considered as a single independent muscle line of action. The actual number of elements depends on the shape of origin and insertion and the muscle architecture, as recorded

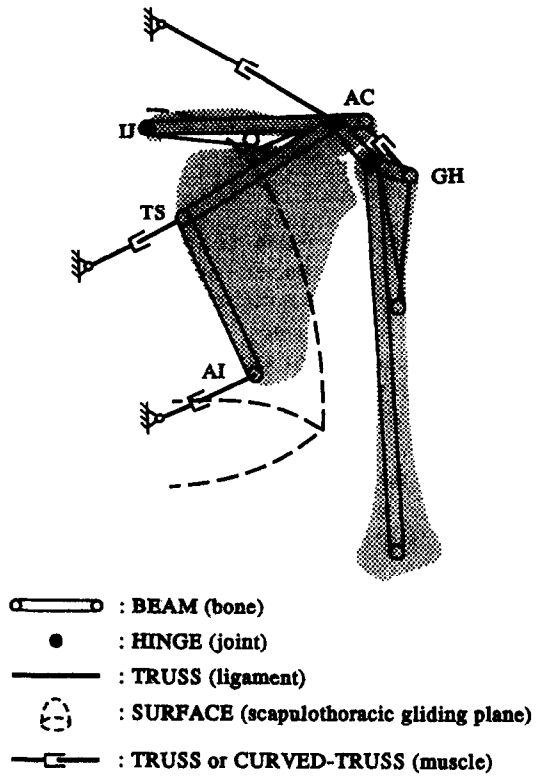

Fig. 3. The shoulder mechanism described by finite elements. Only one ligament and a few muscle elements are shown.

in the cadaver experiment. A general theory for this partitioning of the complete muscle into muscle elements and the coordinates of the attachments has been presented in van der Helm and Veenbaas (1991). An equal share of the PCSA recorded for the whole muscle is attributed to each element. Muscle properties like passive forces, active force–length and force–velocity relationships can easily be added to the TRUSS element. However, due to lack of data on muscle properties only the active force–length relationship is used for simulations (see the results section). Passive forces as obtained on normalized muscle models mainly derived from animal and human leg muscles resulted in huge passive forces due to the extreme lengthening (up to 167%). Until more specific data become available, it is assumed that passive forces do not play a major role. In this study force–velocity dependency is not included since the simulations are of a static nature due to the lack of dynamic data on shoulder motions.

Constraints

In order to achieve a realistic force balance in the shoulder mechanism some other constraints are necessary. Motion constraints of the scapulothoracic gliding plane are modelled by two SURFACE elements. In reality, this constraint can only occur if the scapula is pressed against the thorax. Therefore, the

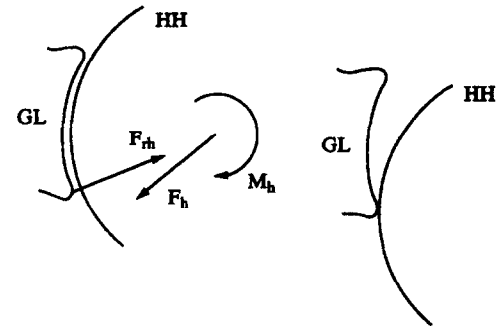

Fig. 4. Resultant force vector $\mathbf{F}_h$ should point to the glenoid, otherwise it cannot be neutralized by the joint reaction force $\mathbf{F}_{rh}$ and the joint will dislocate (GL: glenoid cavity; HH: humeral head).

stress in SURFACE elements is constrained to zero or negative stress (compression). Likewise, the stress in the rigid conoid ligament has been restricted to zero or positive stress (tension). In the glenohumeral joint the resultant force vector should point to the glenoid cavity, otherwise it cannot be neutralized by the joint reaction force and the joint will dislocate (van der Helm *et al.*, 1989); see Fig. 4. The rim of the glenoid has been described as an ellipse. The resultant force vector is constrained to intersect this ellipse (Appendix C). This constraint is implemented as a nonlinear constraint in the optimization procedure.

Input variables

Input variables to the model are positions and motions of the bones. Three-dimensional motion recording of the shoulder girdle is difficult because the scapula and the clavicula move underneath the skin and are not accessible for optical methods but roentgenography. Wallace and coworkers (Wallace, 1982; Wallace and Johnson, 1982) made three-dimensional roentgenographic recordings but unfortunately did not present three-dimensional description of the motions. For an accurate recording the implementation of markers is probably necessary as is done by Peterson *et al.* (1985). However, results of these experiments are not published in detail. Pronk (1987, 1991) and van der Helm and Pronk (1993) used a palpation technique to record three-dimensional positions of bony landmarks of the scapula and the humerus. The position of bony landmarks is used to reconstruct the position and orientation of the bones. A disadvantage of this method is that only static positions of the shoulder mechanism can be recorded. The data published in van der Helm and Pronk (1993) are used for simulations with the model. It should be noted that the limitation to static simulations is caused by available data on scapular positions. The finite element model of the shoulder mechanism allows complete inverse dynamic simulations including velocity and acceleration of the segments.

The choice of adequate generalized coordinates for input is very important. The number of generalized

coordinates is equal to the number of DOF. The shoulder model has seven DOF: four at the shoulder girdle and three at the humerus. In most inverse dynamic simulation studies input variables are the orientation angles of the segments. However, due to the complex motion constraints imposed by the scapulothoracic gliding plane and the clavicula, prescription of the orientation of the scapula results in irrational positions on the thorax. Therefore, position coordinates of bony landmarks are chosen for generalized coordinates, i.e. the y- and z-coordinate of the bony landmark AC (most dorsal point on the AC joint) and the x-coordinate of the bony landmark trigonum spinae (TS). Rotations of the humerus are decomposed as Euler angles in the rotation order pole angle around the global Y-axis, elevation around the local z-axis and axial rotation around the local y-axis (van der Helm and Pronk, 1993). All positions and rotations are described with reference to a global coordinate system with the origin at the incisura jugularis (IJ) and the axes along the anatomical axes (X-axis: medial–lateral; Y-axis: caudal–cranial; Z-axis: ventral–dorsal; right shoulder). The position of the bony landmarks was measured in the cadaver experiments mentioned and thus the recorded motion can be related to the geometry of the cadaver. Position nodes of the bony landmarks are rigidly connected by BEAM elements to the respective bones. Hence, a position change of the bony landmarks will cause a position change of the bones and of all muscle and ligament attachments rigidly connected to these bones.

Axial rotation of the clavicula could not be measured in the palpation experiment. In order to compensate for this missing input variable of the clavicular motion, the number of DOF has been reduced by one through the assumption that the conoid ligament is rigid. Simulations have revealed that only the axial rotation of the clavicula is affected, and that the resulting axial rotation is close to the optimal axial rotation, obtained by minimizing rotations in the AC joint (Pronk, 1991; van der Helm and Pronk, 1993).

Coordinates of the bony landmarks were recorded at 10 subjects during unloaded abduction. The mean orientations of the clavicula and the scapula were derived. Using these mean orientations and the bony dimensions of the cadaver while omitting the motion constraints of the thorax, the desired position coordinates of the bony landmarks were obtained. However, using three of these position coordinates as input variables, the resulting scapular position was slightly changed from the mean orientation, due to the imposed motion constraints of the thorax in the model.

Output variables

The output of the model consists of forces generated by the active elements, subject to an optimization criterion. In addition, joint reaction forces and reaction forces at the scapulothoracic gliding plane are calculated. Validation of the model is severely hampered because none of these forces can be measured directly. Instead, surface EMG recorded at 12 locations is used as an indirect measure of muscle activity.

RESULTS

Kinematics

Figure 5A and B shows the excursion of the scapula over the thorax during humeral abduction, projected on the frontal and the sagittal plane. At 30° abduction, the scapula is oriented towards the plane of humeral elevation by retraction and slightly medial rotation. When the humerus is further abducted, the main rotation of the scapula is lateral rotation in the scapular plane.

Motions of the scapula are important for the excursions of the muscle lines of actions, i.e. the position of the muscle elements. Figure 6A shows the position of the six muscle elements of the scapular part of m. trapezius at 0° humeral abduction. The location of these elements is derived from measurements of origin and insertion including the muscle architecture. Figure 6B shows the same six elements at 180° abduction. The elements are decreased in length and, more clearly, the orientation of the elements with respect to each other and to the articulations has been changed. This implies that the moment arms with respect to the rotation centers of the joints have been changed as well.

Inverse dynamics

As stated in the model of the shoulder mechanism section, an optimization procedure is applied to de-

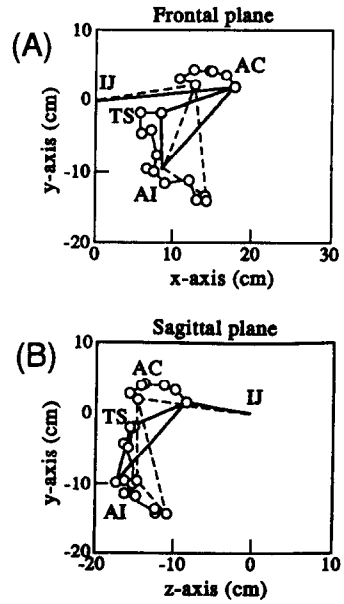

Fig. 5. Position of the scapula (bony landmarks AC, TS and AI) and clavicula (bony landmarks IJ and AC) during humeral abduction at 0° (——) and 180° (– – –). Small circles indicate intermediate positions. A: projection frontal plane; B: projection sagittal plane.

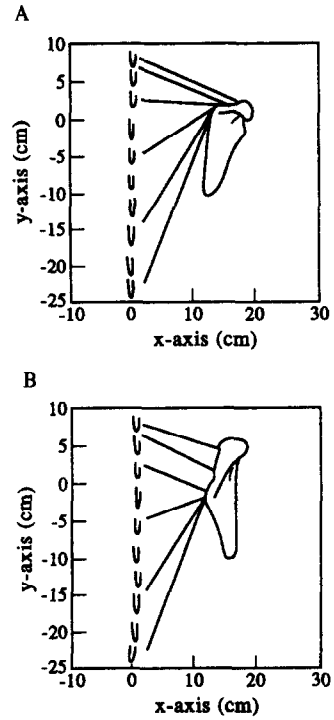

Fig. 6. Position of six TRUSS elements describing the mechanical effect of m. trapezius, scapular part (dorsal view). A: 0° humeral abduction (rest position); B: 180° humeral abduction.

rive a unique vector of muscle stresses σ^{c2} from the motion equations. Stress in a muscle element results in traction forces at its endnodes, exactly as is the case during muscle contraction. One unit of muscle stress results then in one unit of force. The optimization criterion is composed of the stresses σ^{c2} in the active TRUSS and CURVED-TRUSS elements; the results are hereafter presented as muscle forces at the attachments. Four different optimization criteria have been used.

(a) Minimization of the sum of quadratic muscle forces: min $\sum F^2$. Since in the finite element model one unit of stress in the muscle element corresponds to one unit of force exerted at the attachment, this criterion has been implemented as min $\sigma^{c2T} \cdot \sigma^{c2}$.

(b) Minimization of the sum of quadratic muscle stresses: min $\sum (F/\mathrm{PCSA})^2$, where PCSA is the physiological cross-sectional area attributed to each muscle element. Analogously to criterion (a) this criterion has been implemented as min $(\sigma^{c2}/\mathrm{PCSA})^T \cdot (\sigma^{c2}/\mathrm{PCSA})$.

(c) Minimization of the sum of quadratic muscle forces, normalized to the maximal muscle force $F_i\mathrm{max}$ which is a function of PCSA and length of the muscle: min $\sum (F_i/F_i\mathrm{max})^2$ where $F_i\mathrm{max} = \mathrm{PCSA}_i \cdot g(l)$, and $g(l)$ is a function describing the force–length relation of the muscle (Woittiez, 1984). This criterion has been implemented as min $\sum (\sigma_i/\sigma_i\mathrm{max})^2$.

(d) Minimization of the maximal muscle stress in the entire mechanism: min max$(F_1/\mathrm{PCSA}_1, F_2/\mathrm{PSCA}_2, \ldots, F_i/\mathrm{PCSA}_i, \ldots, F_N/\mathrm{PCSA}_N)$, which has been implemented as min max$(\sigma_1/\mathrm{PCSA}_1, \sigma_2/\mathrm{PSCA}_2, \ldots, \sigma_i/\mathrm{PCSA}_i, \ldots, \sigma_N/\mathrm{PCSA}_N)$.

As an example, Fig. 7A–O shows results for all muscles using criterion (b). For comparison, all the results are presented with the same vertical axis. However, the number of elements per muscle should be noted in order to get an impression of the total force exerted by the whole muscle (Table 2).

Special attention is paid to the force and moment balance of the glenohumeral joint. The resulting force vector is constrained to point from the rotation center of the glenohumeral joint to the glenoid cavity. If the constraint is working, in this simulation at 0 and 30° of humeral abduction, especially the antagonistic muscles of the rotator cuff become active. The force output of all other muscles is hardly affected, but the location and the small moment arms of the rotator cuff favor these muscles to deliver the force to keep the humeral head in its socket.

For a few positions of the shoulder mechanism the weight of the arm and counterbalancing muscle forces would result in a dilatation of the trigonum spinae from the scapulothoracic gliding plane. The combined action of the m. rhomboideus and the m. serratus anterior preserves the scapula from losing contact with the thorax, which would be a very unstable situation. This constraint becomes more important with higher loads and during other motions like anteflexion.

EMG–force comparison

Verification of such a complex model of the shoulder mechanism is a cumbersome item. Calculated muscle forces are presumably affected to a large extent by the cadaver morphology. In addition, individual motions are influenced by the underlying morphology. Hence, in this study, verification is limited to comparing muscle forces, using a more or less 'average' cadaver with averaged motions as input, with averaged EMG recordings. In future, the sensitivity of calculations to morphology parameters will be investigated using recorded data of other cadavers. In 12 subjects, eight of them also acted in the palpation experiment, surface EMG was measured at 12 well-defined spots (Table 3), subsequently rectified and averaged for each position. In addition, EMG was averaged over subjects, yielding standard deviations up to 25% of the mean amplitude, which seems to be normal in shoulder muscle EMG (Kronberg, 1989). For each spot, EMG amplitude has been compared with the force output of the nearby muscle element as calculated using the four optimization criteria. A first inspection of EMG patterns revealed for almost all muscles a monotonously increasing amplitude during abduction, in contrast to the muscle forces which peaked at 90° abduction, as would be expected. In the literature, similar EMG patterns are found during humeral abduction (e.g. Inman *et al.*, 1944; Saha, 1961). Kronberg (1989) presented parabolic curves,

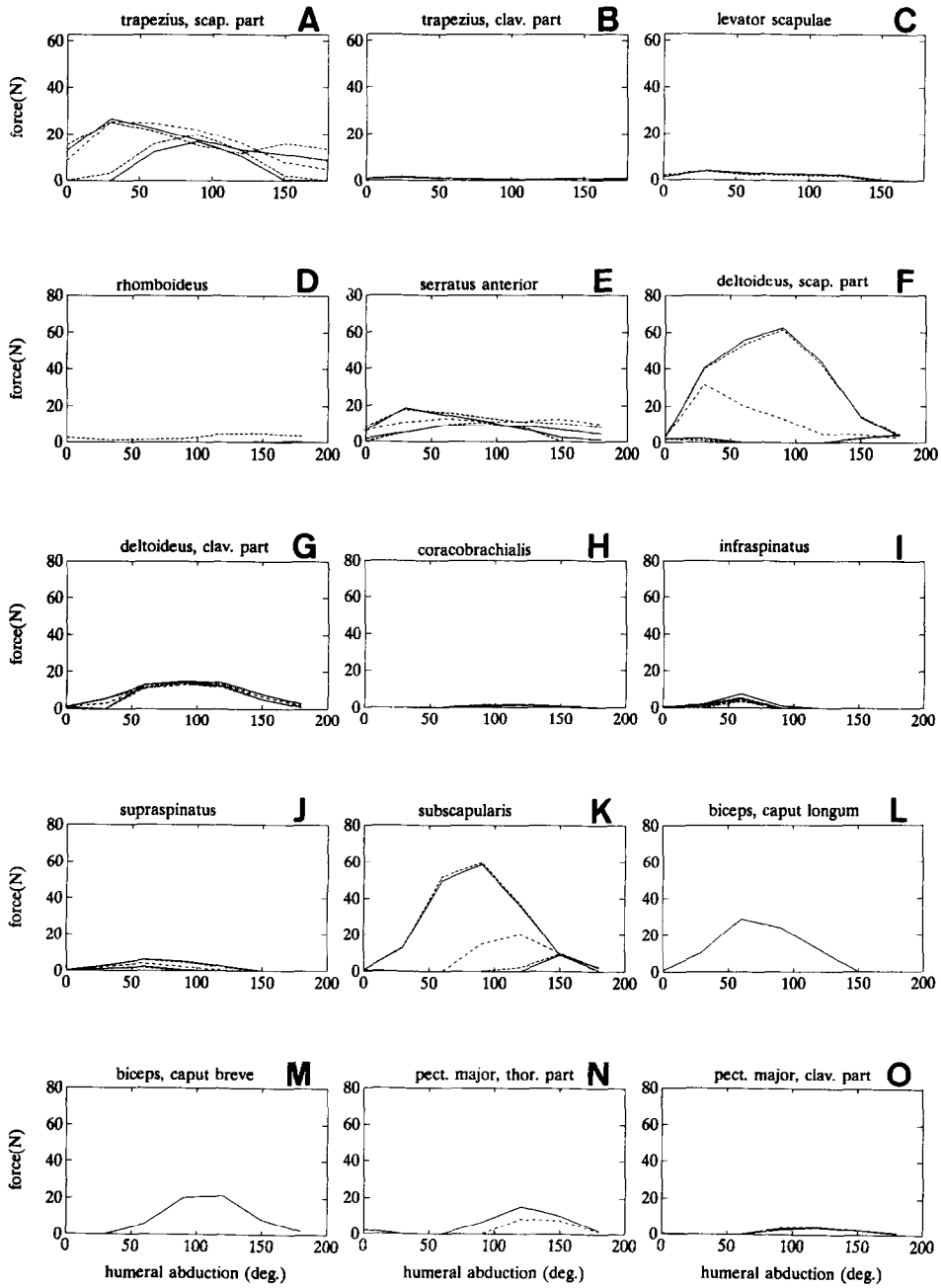

Fig. 7. Muscle force during humeral abduction from 0 to 180°, calculated by minimizing the sum of quadratic muscle stresses. Each line represents the force in a muscle element.

but still EMG amplitude is much higher at 180° abduction than at 0°. Clearly, for EMG amplitude not only is the exerted muscle force a determining factor, but also the muscle length at which EMG is recorded (Heckathorne and Childress, 1981).

Two ways exist to include this length dependency in the verification of the model. Firstly, it can be assumed that the maximal EMG does not depend on muscle length and that it is related with the maximal force output for each muscle length. The ratio between the recorded EMG and the overall maximal EMG can be compared with the ratio between the calculated muscle force and the maximal muscle force at the specified muscle length. Secondly, at each abduction angle in the EMG experiment maximal force output and maximal EMG were recorded. This value will be referred to as local EMG_{max}. But now the problem arises that at maximal force output not necessarily all active muscles are maximally active. During humeral abduction many muscles are solely active in stabilizing the scapula and the humerus and not in contributing to the maximal force output. However,

Table 2. PCSA in cm^2, number of 'active' TRUSS or CURVED-TRUSS elements and PCSA per element (cm^2) for 20 muscles and muscle parts of the shoulder mechanism

Muscle	PCSA	No. of elements	PCSA/element
m. trapezius, scapular part	14.34	6	2.39
m. trapezius, clavicular part	3.12	6	0.52
m. levator scapulae	3.44	3	1.15
m. pectoralis minor	3.43	4	0.86
m. rhomboideus	7.57	3	2.52
m. serratus anterior	11.43	6	1.91
m. deltoideus, scapular part	16.58	6	2.76
m. deltoideus, clavicular part	8.07	6	1.35
m. coracobrachialis	3.20	6	0.53
m. infraspinatus	8.17	6	1.36
m. teres minor	3.10	6	0.52
m. teres major	12.56	6	2.09
m. supraspinatus	4.69	6	0.78
m. subscapularis	14.99	6	2.50
m. biceps, caput longum	1.72	1	1.72
m. biceps, caput breve	1.78	1	1.78
m. triceps, caput longum	6.24	2	3.12
m. latissimus dorsi	8.52	5	1.70
m. pectoralis major, thoracic part	8.68	5	1.74
m. pectoralis major, clavicular part	3.55	5	0.71

Table 3. Electrode positions for surface EMG recordings

Muscle	Electrode position
m. trapezius, p. descendens	In a vertical line above trigonum spinae (TS), 2 cm below the edge of the muscle
m. trapezius, p. transversalis	1 cm medial and 4 cm cranial to TS
m. trapezius, p. ascendens	2/3 on the line between TS and the eighth thoracal vertebra (T8), 4 cm from the edge of the muscle
m. deltoideus, p. anterior	2 cm below the anterior rim of the acromion
m. deltoideus, p. medialis	2 cm below the lateral rim of the acromion
m. deltoideus, p. posterior	2 cm below angulus acromialis
m. infraspinatus	In the middle of TS and angulus inferior (AI), 2 cm of the medial border of the scapula
m. serratus anterior	Roughly the sixth head at the level of the nipple, just lateral to the m. pectoralis major
m. latissimus dorsi	6 cm below AI
m. pectoralis major, p. clav.	In the middle of the sternoclavicular joint and processus coracoideus, 2 cm below the clavicula
m. pectoralis major, p. thor.	6 cm above the nipple
m. biceps, caput breve and longum	In the midst of the muscle

with the shoulder model the maximal force output can be simulated as well. The ratio between recorded EMG and local EMG_{max} can be compared with the ratio between calculated muscle force and muscle force calculated at maximal force output.

Both methods have been applied in the shoulder model, but neither of them gave the desired results. Despite normalization, EMG amplitude curves were still monotonously increasing, whereas the normalized muscle forces had a peak around 90° abduction. Maximal EMG depends on muscle length (Heckathorne and Childress, 1981), the optimum muscle length is probably not at the initial length and the width of the force–length relation is unknown. It is concluded that no EMG–force relation can be assessed without accounting for change of muscle length, which hampers the use of surface EMG (Mouton *et al.*, 1991). Apparently, only on–off patterns of recorded EMG can be used for verification of the model. However, humeral abduction is not a cyclic motion like walking or cycling, and most muscles are active throughout the motion. Figure 8 shows the results of the four different optimization criteria for 12 muscles. Figure 9 shows the EMG patterns of these muscles as a percentage of the maximal EMG. It is concluded that results of the model simulations reasonably correspond to recorded EMG patterns, based on an on–off comparison, but that the verification is merely qualitative and no distinction between the four criteria could be made.

Criterion (d), minimization of the maximal muscle stress, appeared to be a numerically unstable cri-

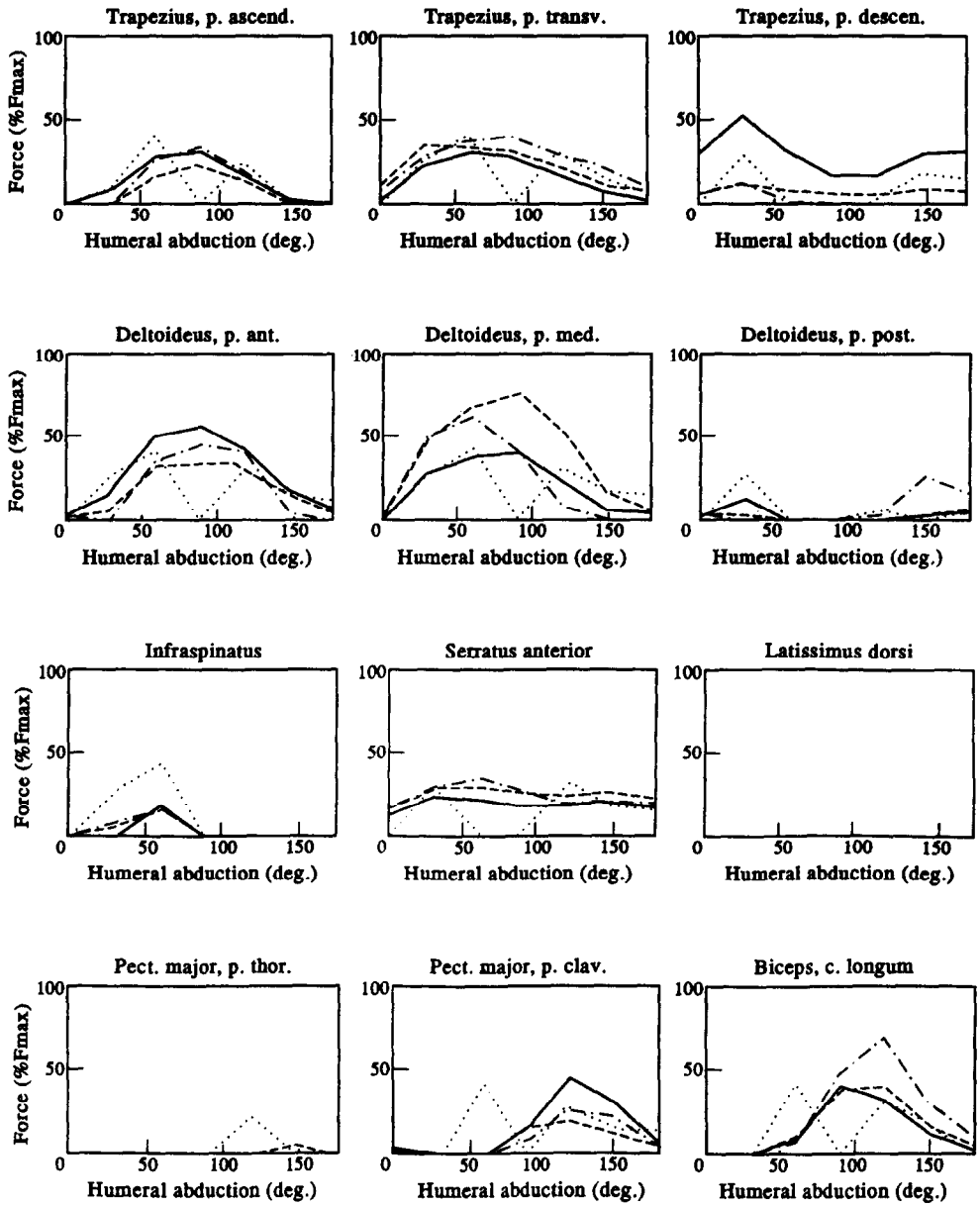

Fig. 8. Muscle forces (as percentage of maximal muscle force) calculated with four different optimization criteria. (——): min $\sum F^2$; (. . . . .): min $\sum (F/\text{PCSA})^2$; (– – –): min $\sum (F_i/F_i\text{max})^2$; (–·–·–): min $(\max(F_1/)\text{PCSA}, \ldots, F_i/\text{PCSA}_i, \ldots, F_N/\text{PCSA}_N)$.

terion. At 0 and 90° humeral abduction, no solution was found for the indeterminacy problem. At 90° humeral abduction the muscle stress needed around the glenohumeral joint exceeded the muscle stress needed for the thoracoscapular muscles. No load sharing between these two muscle groups could be provided by, e.g. a muscle with a suitable location which crosses all three joints. Hence, the load sharing problem between the thoracoscapular muscles is still unresolved, and no solution for the entire system has been found. In the initial position (0° humeral abduction) a similar problem occurred, but in this position the stress in the thoracoscapular muscles exceeds the stress in the glenohumeral muscles.

DISCUSSION

Even if a model is considered to be a simplification of the real system, a model of such a complex system as the shoulder mechanism still remains a very complex model. This complexity is probably the reason why hardly any models exist.

The finite element method as presented in this paper is a very powerful tool for musculoskeletal modelling, allowing the development of all kinds of mechanisms. Elements are easily added or removed. The choice of input variables can be changed as well as the position coordinates of morphological structures. The basic elements combined with the special-purpose ele-

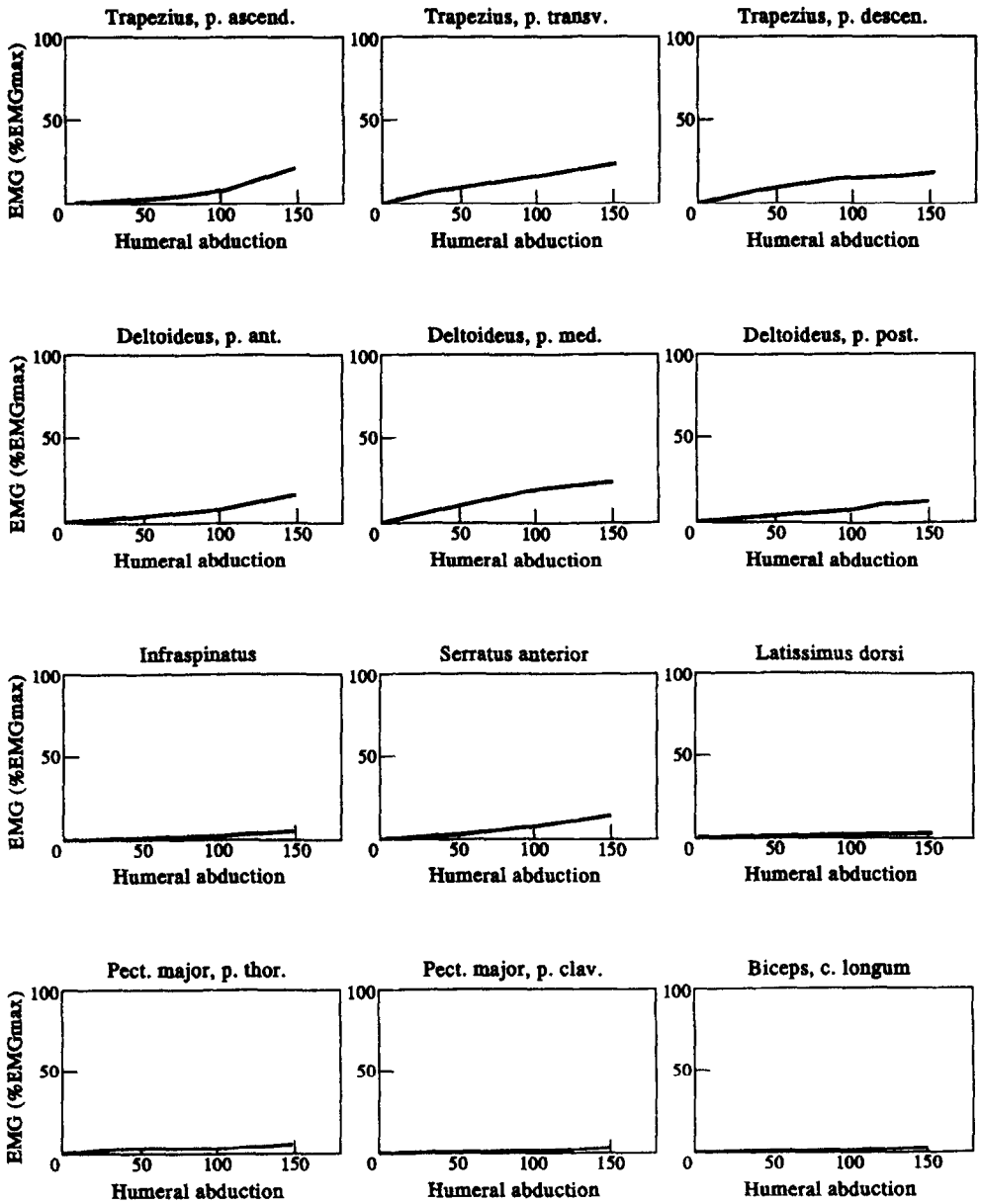

Fig. 9. Surface EMG (percentage of maximal EMG) of a number of muscles of the shoulder mechanism.

ments provide modelling of all important morphological structures to be represented.

Building an integral model of the shoulder mechanism is essential for analyzing the function of morphological structures. It gives a complete picture of the shoulder motion and the muscle action, instead of isolating small parts and neglecting the influence of separate parts on each other. In fact, the finite element model of the shoulder mechanism as presented in this paper very much resembles the physical model as built by Mollier (1899); see Fig. 1. Length changes of the muscles can be calculated from motion of the bones, and, in reverse order, when the length of a muscle is prescribed, the resulting motion can be calculated. But, in addition, the finite element model is (inverse) dynamic, i.e. the force in the muscles can be calculated subject to the motion and external load of the mechanism. A new theory was developed for adequately representing the mechanical effect of muscles with large attachment sites with a limited number of muscle lines of action (van der Helm and Veenbaas, 1991). In the model each muscle line of action is represented by an active, force generating element between origin and insertion. These elements can be straight or curved around a bony contour. In the inverse dynamic analysis no stiffness is attributed to ligaments, since the recorded input motion was not accurate enough for assessing the deformation of the

ligaments and incorrect deformations could consequently result in extremely large stresses in the ligaments and hence in the whole mechanism. Thus, only the length change of ligaments can be analyzed. The conoid ligament was chosen to have infinite stiffness (rigid). Evidently, there is no length change, but forces can be transmitted from the scapula to the clavicula through the ligament. Included in the constraints of the optimization procedure, only traction forces are allowed in this ligament.

Furthermore, important aspects are included as the constraint imposed by the scapulothoracic gliding plane, rendering the system a closed-chain mechanism, and the necessary stability of the glenohumeral joint. The restriction to compression forces in the gliding plane results in additional forces in mainly the m. rhomboideus and the m. serratus anterior, pulling the scapula to the thorax. In fact, when the constraint is working, the activity of these muscles is still underestimated because at zero compression force the scapula is not sufficiently stabilized: external and internal disturbances could easily cause the scapula to lose contact, which would result in a limited positioning ability for the entire upper extremity.

Due to the lax capsule and small articulating surface of the glenoid cavity, the glenohumeral joint can easily dislocate. Muscle forces are essential for controlling the stability of the joint. The resultant force vector is constrained to pass from the rotation center through the articular surface of the glenoid cavity. If this vector would point outside the glenoid cavity it could not fully be counteracted by the joint reaction force vector, and a dislocating force would result; see Fig. 4 (van der Helm *et al.*, 1989). This constraint mainly influences the force generated by muscles of the rotator cuff. Without this constraint these muscles are hardly active, due to optimization criteria which favor muscles with large moment arms. If the constraint is working the rotator cuff becomes active, because pointing the resultant force vector requires antagonistic muscle forces and then muscles with smaller moment arms are favored. As a matter of fact, in the model, the activity of the rotator cuff muscles is underestimated because the resultant force vector is allowed to point anywhere within the glenoid cavity. It is doubtful whether a stable position of the glenohumeral joint is achieved when the joint reaction force vector points towards the rim of the glenoid. Adjusting the joint reaction force vector towards the midst of the glenoid cavity requires large forces of the rotator cuff muscles, proportional to the magnitude of the joint reaction force vector. Nevertheless, thus far in all musculoskeletal models it is assumed that calculated joint reaction forces are counteracted by joint structures as ligaments and the shape of articular surfaces. It is not likely that this is always true. In the glenohumeral joint, with its lax capsule and spherical shape of the articular surface, the orientation of the joint reaction force, which prevents dislocation, is easily calculated. Sometimes additional muscle force is required to maintain stability. It can be concluded that for all joints in the human body this stability requirement should be considered, which will probably shed new light on the role of muscles with small moment arms.

Any model is as good as its validation. Validation generally requires a comparison of the predicted output of the model with the measured output of the system. One problem of validating musculoskeletal models is that the predicted output, muscle forces, cannot be measured directly. Normally only the external moment delivered by a number of muscles can be measured, which can only be decomposed into individual muscle forces using a musculoskeletal model. Therefore, the strict requirements for validation of the model are not fulfilled. Only verification of the model is possible, i.e. determine whether the predicted behavior of the model agrees qualitatively with the recorded output. One method of assessing the individual contribution of muscles is to compare predicted muscle force with recorded EMG. In this study surface EMG was recorded at 12 locations in the shoulder mechanism. Formally, verification of the force output of 95 muscle elements with a subset of 12 recorded signals would not be sufficient. However, if these 12 signals agree, the other 83 signals will be assumed to be similarly accurate due to the large interactions in the system.

In this study four different optimizing criteria are used to calculate muscle forces. A comparison of the results with EMG amplitude should offer the opportunity to distinguish between these criteria. However, the comparison is hampered by the fact that EMG is length dependent (Heckathorne and Childress, 1981). Length changes range from 52 to 167% with respect to initial length at 0° humeral abduction, contrasting with published force–length relationships ranging from about 60 to 140% of the optimum length (Woittiez, 1984). To eliminate length dependency one method is to normalize the calculated muscle force to the maximal force estimated using the force–length relationship. Another method is to normalize the EMG to the local maximal EMG. In both cases comparison failed because the optimum muscle length in the force–length relation is unknown. Despite normalization with length-dependent measures, the relation between normalized EMG and muscle force remains obscure. More fundamental EMG studies have to be performed to analyze length dependency and, in addition, optimum muscle length *in vivo* needs to be assessed. Meanwhile, verification of the shoulder model is limited to specific features, based more on on–off comparisons than on quantitative comparisons with the EMG amplitude. As shown in Figs 8 and 9, similarity between force patterns and EMG is, for most muscles, reasonable. EMG amplitude is subject to measurement errors, length and velocity effects. Hence, it is not very reliable for muscle force predictions. Model calculations provide insight into the mechanical behavior of the shoulder mechanism and

muscle forces in particular, although they are affected by modelling assumptions and parameters. It is difficult to compare model calculations with any recording of the mechanical behavior of the shoulder mechanism.

Since more muscle elements are present than motion equations, the system is indeterminate. An optimization criterion is necessary which preferably reflects the physiological criterion the central nervous system uses to control muscle forces. Criterion (a), minimization of quadratic muscle forces, gives incorrect results, because this criterion does not account for the stress in the muscle, denoted by the PCSA, which leads to an overuse of favorably located muscles. In addition, this criterion is very sensitive to the number of muscle lines of action used to represent the muscle, just because the PCSA is not included in the criterion. Criterion (b), minimization of the sum of squared muscle stresses, distributes the necessary muscle forces partly according to the PCSA. However, even using this criterion, some muscle elements which have an excellent moment arm will be favored to a large extent, e.g. m. deltoideus, scapular part, and m. subscapularis. Criterion (c) includes the effect of the force–length relationship. A disadvantage is that the muscle optimum length is unknown *in vivo* and, in addition, considering the large length changes of the muscles (52–167%), the force–length relationship needs to be re-evaluated. The last criterion, minimization of the maximal muscle stress in the mechanism, prevents the calculation of extremely high muscle stresses. A disadvantage of this criterion is that it is numerically unstable, since the DOF of the scapula and humerus are sometimes not sufficiently related to each other.

Criteria (b)–(d) do not show much differences. With the help of EMG it could not be distinguished which of these optimization criteria provides the best muscle force predictions. Considering the computational efficiency, criterion (b), minimization of the sum of squared muscle stresses, has our preference. However, since the physiological way in which muscle forces are distributed over the system is still unknown, and is presumably to a large extent subject to task requirements, it could be possible that none of the mathematical criteria used in this study provides adequate muscle force calculations.

CONCLUSIONS

(1) The finite element method as used in the computer program SPACAR is very much suited for complex musculoskeletal models as the shoulder mechanism.

(2) A detailed model of the shoulder mechanism has been developed which can provide excellent insight into the function of morphological structures.

(3) Constraints imposed by the scapulothoracic gliding plane are important for the motions and force balance of the shoulder girdle.

(4) EMG amplitude is a poor measure to validate musculoskeletal models. Only on–off patterns can be compared.

(5) Rotator cuff muscles are active in controlling the stability of the glenohumeral joint by pointing the resultant force vector to the articular surface of the glenoid.

Acknowledgements—The help of Hein Daanen and Monique van der Hoeven in conducting the EMG experiment is greatly acknowledged.

REFERENCES

An, K. N., Takahashi, K., Harrigan, T. P. and Chao, E. Y. (1984) Determination of muscle orientations and moment arms. *J. biomech. Engng* **106**, 280–282.

DeLuca, C. J. and Forrest, W. J. (1973) Force analysis of individual muscles acting simultaneously on the shoulder during isometric abduction. *J. Biomechanics* **6**, 385–393.

Dul, J. (1987) Shoulder muscle load during work with elevated arms. In *Proc. 11th ISB-Congr., Biomechanics XI-A* (Edited by de Groot, G., Hollander, A. P., Huijing, P. A. and van Ingen Schenau, G. J.), pp. 471–476. Free University Press, Amsterdam.

Grossmann, W. (1976) *Geodatische Rechnungen und Abbildungen in der Landesvermessung*. Verlag Konrad Wittwer, Stuttgart.

Heckathorne, C. W. and Childress, D. S. (1981) Relationships of the surface electromyogram to the force, length, velocity, and contraction rate of the cineplastic human biceps. *Am. J. Phys. Med.* **60**, 1–19.

Hvorslev, C. M. (1927) Studien ueber die Bewegungen der Schulter. *Skand. Arch. Physiol.*, separatabdruck.

Inman, V. T., Saunders, J. B. and Abbott, L. C. (1944) Observations on the function of the shoulder joint. *J. Bone Jt Surg.* **26A**, 1–30.

Jonker, B. (1988) A finite element dynamic analysis of flexible spatial mechanisms and manipulators. Doctoral thesis, Delft University of Technology, The Netherlands.

Karlsson, D. (1990) Predictions of the muscle activity in the human shoulder. *Abstr. 1st World Congr. Biomech.*, San Diego, Vol. II, p. 162.

Karlsson, D. and Peterson, B. (1992) Towards a model for force predictions in the human shoulder. *J. Biomechanics* **25**, 189–199.

Karlsson, D., Peterson, B., Hogfors, C. and Herberts, P. (1989) In *Proc. 12th ISB Congr.*, Los Angeles (Edited by Gregor, R. J., Zernicke, R. F. and Whiting, W. C.), pp. 684–685.

Kronberg, M. (1989) Muscle activity and coordination in the normal shoulder: an electromyographic study. Doctoral thesis, Sweden.

Mollier, S. (1899) Ueber die Statik und Mechanik des menslichen Schultergurtels unter normalen und pathologische Verhaltnissen. Festschrift für C. v. Kupfer, Jena.

Mouton, L. J., Hof, A. L., de Jongh, H. J. and Eisma, W. H. (1991) The influence of posture on the relation between surface EMG amplitude and back muscle moment; consequences for the use of surface EMG to measure backload. *Clin. Biomech.* (accepted).

Peterson, B., Hogfors, C., Herberts, P., Selvik, G. and Sigholm, G. (1985) The shoulder rhythm. *Abstract Book: 218, 10th ISB-Congr.*, Umea, Sweden.

Poppen, N. K. and Walker, P. S. (1978) Forces at the glenohumeral joint in abduction. *Clin. Orthop. Rel. Res.* **135**, 165–170.

Pronk, G. M. (1987) Three-dimensional determination of the position of the shoulder girdle during humerus elevation. In *Proc. 11th ISB-Congr., Biomechanics XI-B* (Edited by

de Groot, G., Hollander, A. P., Huijing, P. A. and van Ingen Schenau, G. J.), pp. 1070–1076. Free University Press, Amsterdam.
Pronk, G. M. (1989) A kinematic model of the shoulder girdle: a resume. *J. Med. Engng Technol.* **13,** 119–123.
Pronk, G. M. (1991) The shoulder girdle: analysed and modelled kinematically. Doctoral thesis, Delft University of Technology, The Netherlands.
Pronk, G. M. and van der Padt, A. (1986) The modelling of the scapulothoracic wall. Rep. N-245, Lab. WBMR, Delft University of Technology, The Netherlands.
Saha, A. K. (1961) *Theory of Shoulder Mechanism: Descriptive and Applied.* Charles C. Thomas, Springfield, IL.
Schwab, A. L. (1983) Dynamics of mechanisms with flexible links. Rep. A-758, Lab. WBTM, Delft University of Technology, The Netherlands (in Dutch).
Shampine, L. F. and Gordon, M. K. (1975) *Computer Solution of Ordinary Differential Equations, the Initial Value Problem.* W. J. Freeman, San Francisco, CA.
Shiino, K. (1913) Schultergelenkbewegungen und Schultermuskelarbeit. *Arch. Anat. Physiol.* (Suppl. Anat. Abtig.) 1–88.
Sol, E. J. (1983) Kinematics and dynamics of multibody systems: a systematic approach to systems with arbitrary connections. Doctoral thesis, Eindhoven University of Technology, The Netherlands.
van der Helm, F. C. T. (1993) Calculation of muscle lines of action wrapped around bony contours. *J. Biomechanics* (submitted).
van der Helm, F. C. T. and Pronk, G. M. (1993) Three-dimensional recording and description of the motions of the shoulder mechanism. *J. Biomech. Engng* (accepted).
van der Helm, F. C. T., Pronk, G. M., Veeger, H. E. J. and van der Woude, L. H. V. (1989) The rotation center of the glenohumeral joint. In *Proc. 12th ISB Congr.*, Los Angeles (Edited by Gregor, R. J., Zernicke, R. F. and Whiting, W. C.), pp. 676–677.
van der Helm, F. C. T., Veeger, H. E. J., Pronk, G. M., van der Woude, L. H. V. and Rozendal, R. H. (1992) Geometry parameters for musculoskeletal modelling of the shoulder mechanism. *J. Biomechanics* **25,** 129–144.
van der Helm, F. C. T. and Veenbaas, R. (1991) Modelling the mechanical effect of muscles with large attachment sites: application to the shoulder mechanism. *J. Biomechanics* **24,** 1151–1163.
Veeger, H. E. J., van der Helm, F. C. T., van der Woude, L. H. V., Pronk, G. M. and Rozendal, R. H. (1991) Inertia and muscle contraction parameters for musculoskeletal modelling of the shoulder mechanism. *J. Biomechanics* **24,** 615–629.
Wallace, W. A. (1982) The dynamic study of shoulder movements. In *Shoulder Surgery* (Edited by Bailey, I. and Kessel, L.), pp. 139–143. Springer, Berlin.
Wallace, W. A. and Johnson, F. (1982) A biomechanical appraisal of the acromioclavicular joint. In *Shoulder Surgery* (Edited by Bailey, I. and Kessel, L.), pp. 179–182. Springer, Berlin.
van der Werff, K. (1977) Kinematic and dynamic analysis of mechanisms: a finite element approach. Doctoral thesis, Delft University of Technology, The Netherlands.
van der Werff, K. and Jonker, B. (1983) Dynamics of flexible mechanisms. In *Proc. NATO Advanced Study Inst. on Computer Aided Analysis and Optimization of Mechanical System Dynamics*, Iowa City, pp. 381–400.
Winters, J. M. and Stark, L. (1985) Analysis of fundamental human movement patterns through the use of in-depth antagonistic muscle models. *IEEE Trans. biomed. Engng* **32,** 826–839.
Woittiez, R. (1984) A quantitative study of muscle architecture and muscle function. Doctoral thesis, Free University Amsterdam, The Netherlands.
Wood, J. E., Meek, S. G. and Jacobsen, S. C. (1989) Quantification of human shoulder anatomy for prosthetic arm control. I. Surface modelling. *J. Biomechanics* **22,** 309–325.

APPENDIX A

The SURFACE element has one position node and one deformation mode: the distance between the position node and the predefined surface, i.e. an ellipsoid representing the thorax with its axes along the main axes of the coordinate system. The equation of such an ellipsoid with center $\mathbf{M}(m_x, m_y, m_z)$ and axes a_x, a_y and a_z for each point $\mathbf{I}(x, y, z)$ on the surface is

$$\left[\frac{x-m_x}{a_x}\right]^2+\left[\frac{y-m_y}{a_y}\right]^2+\left[\frac{z-m_z}{a_z}\right]^2=1. \tag{A1}$$

The distance is calculated along the normal vector $\mathbf{N}$ of the ellipsoid through the position node $\mathbf{P}(P_x, P_y, P_z)$, intersecting the ellipsoid at $\mathbf{P}'(P'_x, P'_y, P'_z)$. The line through the points P and P' is described by

$$\begin{bmatrix}P_x\\P_y\\P_z\end{bmatrix}=\begin{bmatrix}P'_x\\P'_y\\P'_z\end{bmatrix}+\mu\cdot\mathbf{N}=\begin{bmatrix}P'_x\\P'_y\\P'_z\end{bmatrix}+\mu\cdot\begin{bmatrix}\frac{2(P'_x-m_x)}{a_x^2}\\[2pt]\frac{2(P'_y-m_y)}{a_y^2}\\[2pt]\frac{2(P'_z-m_z)}{a_z^2}\end{bmatrix}. \tag{A2}$$

Combining equations (A1) and (A2) results in function $F(\mu)$:

$$F(\mu)=\left[\frac{P_x-m_x}{a_x-2\mu/a_x}\right]^2+\left[\frac{P_y-m_y}{a_y-2\mu/a_y}\right]^2+\left[\frac{P_z-m_z}{a_z-2\mu/a_z}\right]^2-1. \tag{A3}$$

The parameter μ can be solved numerically from this equation when $F(\mu)$ is zero, and with equation (A2) the coordinates of $\mathbf{P}'$ can be calculated. Consequently, the distance between $\mathbf{P}$ and $\mathbf{P}'$ is the distance from $\mathbf{P}$ to the ellipsoid:

$$\varepsilon_1=\|\mathbf{P}-\mathbf{P}'\|. \tag{A4}$$

The 3×1 vector of first derivatives is the normal vector $\mathbf{N}$ to the ellipsoid through $\mathbf{P}'$, normalized to a unit vector,

$$\frac{\delta\varepsilon_1}{\delta\mathbf{P}}=\frac{\mathbf{N}}{\|\mathbf{N}\|}, \tag{A5}$$

and the 3×3 matrix of second derivatives is

$$\frac{\delta^2\varepsilon_1}{\delta\mathbf{P}\cdot\delta\mathbf{P}^{\mathrm{T}}}=\mathbf{I}-\left(\frac{\mathbf{N}}{\|\mathbf{N}\|}\cdot\frac{\mathbf{N}^{\mathrm{T}}}{\|\mathbf{N}\|}\right). \tag{A6}$$

APPENDIX B

The CURVED-TRUSS element describes the mechanical effect of a TRUSS element between two position nodes $\mathbf{P}_1$ and $\mathbf{P}_2$, which is wrapped around a predefined surface. $\mathbf{P}_2$ is attached to the same rigid body as the surface. The tangent points $\mathbf{R}_1$ and $\mathbf{R}_2$ of the shortest line between $\mathbf{P}_1$ and $\mathbf{P}_2$ around the surface can be calculated (Fig. B1). The CURVED-TRUSS element has three position nodes, $\mathbf{P}_1$, $\mathbf{P}_2$ and $\mathbf{R}_1$, and one deformation mode, elongation. The deformation is calculated analogously to the TRUSS element:

$$\varepsilon_1=\|\mathbf{P}_1-\mathbf{R}_1\|+a(\mathbf{R}_1,\mathbf{R}_2)+\|\mathbf{R}_2-\mathbf{P}_2\|-l_0, \tag{B1}$$

where $a(\mathbf{R}_1, \mathbf{R}_2)$ denotes the distance between $\mathbf{R}_1$ and $\mathbf{R}_2$ over the surface and l_0 is the initial length of the element. Shortening (or lengthening) and force exertion of the CURVED-TRUSS element virtually take place between $\mathbf{P}_1$ and $\mathbf{R}_1$, since $\mathbf{R}_1$, $\mathbf{R}_2$ and $\mathbf{P}_2$ are at the same rigid body. Then, by definition, $\delta\varepsilon_1/\delta\mathbf{P}_2=0$, and the behavior of the CURVED-TRUSS element becomes similar to a straight TRUSS element between $\mathbf{P}_1$ and $\mathbf{R}_1$.

At each step of the mechanism $\mathbf{R}_1$ and $\mathbf{R}_2$ are calculated. The surface is described with respect to the local coordinate

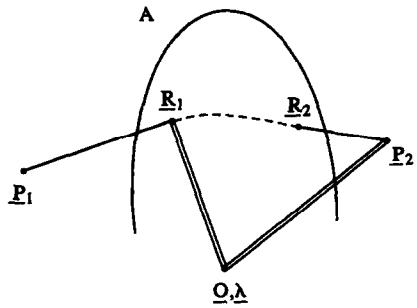

Fig. B1. The CURVED-TRUSS element. $\mathbf{P}_1$ and $\mathbf{P}_2$ are the endnodes. $\mathbf{R}_1$ and $\mathbf{R}_2$ are the tangent points to the surface A. The line through $\mathbf{P}_1, \mathbf{R}_1, \mathbf{R}_2$ and $\mathbf{P}_2$ is the shortest line between $\mathbf{P}_1$ and $\mathbf{P}_2$ over the surface A. $\mathbf{P}_2$ and $\mathbf{R}_1$ are connected with BEAM elements with the local coordinate system with origin at the position node $\mathbf{O}$ and the orientation defined by the orientation node λ. Surface A is fixed in the local coordinate system.

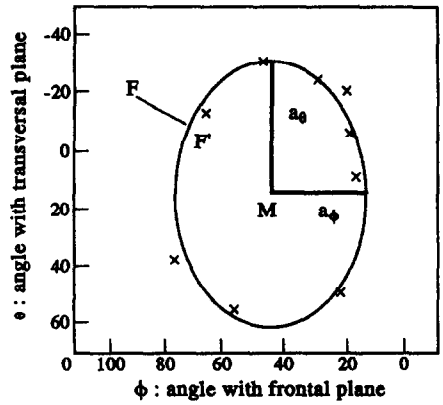

Fig. C1. An ellipsoid with center $\mathbf{M}(\phi_m, \theta_m)$ and axes a_ϕ and a_θ is fitted to the pole coordinates ϕ and θ of the data points ('×') on the rim of the glenoid cavity with respect to the rotation center of the GH joint. The pole coordinates of the resultant muscle force vector $\mathbf{F}(\phi_f, \theta_f)$ are constrained to point inside the ellipsoid.

system of the bone. If the bone is moving, the surface changes position and orientation accordingly. $\mathbf{P}_2$ and $\mathbf{R}_1$ are connected with rigid BEAM elements to the same local coordinate system as the surface. The BEAM connecting $\mathbf{R}_1$ is repositioned each step according to the motion of $\mathbf{R}_1$ with respect to the local coordinate system. In the trivial case where the line through $\mathbf{P}_1$ and $\mathbf{P}_2$ does not intersect the surface, the CURVED-TRUSS element behaves similarly to a straight TRUSS element between $\mathbf{P}_1$ and $\mathbf{P}_2$.

Currently, three types of surfaces are used: a sphere, a cylinder and an ellipsoid. Calculation of the tangent points $\mathbf{R}_1$ and $\mathbf{R}_2$ at these surfaces has been presented in van der Helm (1993).

APPENDIX C

Constraint of the glenohumeral joint

In the cadaver study a sphere was fitted to data points recorded at the articular surface of the glenoid (van der Helm *et al.*, 1992). Data points at the rim of the glenoid were indicated. The direction vector from the center of the sphere to these data points can be described by pole coordinates: a rotation ϕ around the global Y-axis (angle with the frontal plane) and subsequently a rotation θ around the rotated z'-axis (angle with the transversal plane). An ellipsoid with center $\mathbf{M}(\phi_m, \theta_m)$ and axes a_ϕ and a_θ can be fitted to the obtained rotation angles using a least-squares criterion, describing the orientation and shape of the glenoid (Fig. C1). The orientation of the glenoid changes with the motions of the scapula, which is reflected in position changes of center $\mathbf{M}$.

The direction of the resultant joint reaction force vector $\mathbf{F}$ is described by the rotation angles ϕ_f and θ_f. $\mathbf{F}$ is constrained to intersect the glenoid. Hence, the following equation can be derived:

$$\left(\frac{\phi_m - \phi_f}{a_\phi}\right)^2 + \left(\frac{\theta_m - \theta_f}{a_\theta}\right)^2 \leq 1. \qquad \text{(C1)}$$

This equation has been implemented as a nonlinear inequality constraint in the optimization procedure.